·Particle Beams and Accelerator Technology·

Influence of SXFEL resistive wall wakefield on beam phase space distortion*

Gong Youwei[1,2], Cheng Wencai[1,2], Zhao Minghua[1], Li Xuan[3], Gu Duan[3], Zhang Meng[3]

(1. *Shanghai Institute of Applied Physics*, *Chinese Academy of Sciences*, *Shanghai* 201800, *China*;
2. *University of Chinese Academy of Sciences*, *Beijing* 100049, *China*;
3. *Shanghai Advanced Research Institute*, *Chinese Academy of Sciences*, *Shanghai* 201210, *China*)

Abstract: X-ray free-electron laser (XFEL), due to its ultra-high brightness, ultra-short pulse and other characteristics, has been built worldwide. Based on the theory of wakefield, we calculate the resistive wall wakefield from the linear accelerator (linac) exit to the end of the undulator in Shanghai X-ray free electron laser (SXFEL) with bunch traveling through the 245 m stainless steel transfer line and copper beamline in undulator. Then we analyze the resistive wall wakefields which eventually lead to the distortion of the longitudinal phase space within the bunch. Finally, the theoretical predictions of influence of resistive wall wakefield are compared with experiment results on SXFEL, which shows great agreement. The detailed research provides a direction for subsequent FEL optimization.

Key words: SXFEL, longitudinal phase space, resistive wall wakefield, energy distribution distortion

CLC number: TL53 **Document code:** A **doi**: 10.11884/HPLPB202234.210491

X-ray free electron lasers (XFEL) have ushered in a new era of ultrafast X-ray sciences[1-5]. The novel source can provide a few fs and even sub-fs pulses for the nanomaterials science, femtosecond chemistry, biomolecular structure and other fields, but it also faces tremendous challenges for electron beam brightness and lower emittance in bunches. XFEL as the fourth-generation light source has been planned and constructed worldwide. SXFEL, as the first facility working at soft X-ray region in China, has been built at Shanghai Light Source[6-9].

Fig.1 shows the layout of the SXFEL accelerator. The linear accelerator driving the FEL requires precise control of the electron bunch phase space, including compression to high peak currents and providing a flat energy profile along the bunch length. The SXFEL device starts from injector, consisting of the 1.6 cell photocathode RF gun with nearly 500 pC charge per bunch, and following two 3m accelerating structures for beam energy pre-acceleration. The first accelerating pipe accelerates the bunch "off-crest" and generates a nearly linear energy correlation along the bunch to initiate the first stage of compression (chicane). There is a short X-band RF section (X1), following L1, which is used to linearize the compression by removing the quadratic energy-time bunch correlation generated before and resulting in maintaining a uniform temporal distribution along the bunch. Then, the bunch is accelerated and compressed again in L2 and the second chicane. The magnetic compression employed in such FELs typically leaves an undesired time-energy correlation in the bunch (an energy chirp), which can broaden the FEL bandwidth if not compensated properly. Finally, the last accelerator section, is set nearly on-crest, to get 1.5 GeV beam energy and simultaneously cancels the linear correlated energy spread with the strong geometric longitudinal wakefield of the C-band rf-structures[10-11].

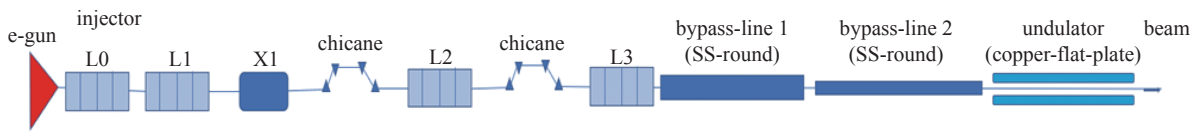

Fig. 1 Layout of the SXFEL

* **Received date:** 2021-11-16; **Revised date:** 2022-03-23
E-mail: Gong Youwei, gongyouwei@sinap.ac.cn.
Corresponding author: Zhang Meng, zhangmeng@zjlab.org.cn.

During the beam transportation from e-gun to main accelerator sections, the longitudinal beam dynamics has been studied[10]. In the downstream, two types of stainless-steel vacuum pipe connect the linac section with a 40 m undulator section. Due to the ultra-short bunch length and long vacuum pipe, the resistive wakefield effect is regarded as a non-negligible and vital influence on the longitudinal phase space.

In this paper, we primarily explore the resistive wall wakefield effects from the exit of the linac to the end of the undulator with three different parameters pipes in SXFEL. In Sec. Ⅱ, longitudinal wakefield in round and flat plate with 1 kA uniform bunch are obtained based on short-range wakefield calculation, and simulation results with fluctuations within the bunch are demonstrated. The beam tests experiment on SXFEL are demonstrated and verified with great consistencies compared with the previous calculation in Sec. Ⅲ. Lastly, a brief conclusion is presented.

1 Wakefield calculation of three different pipes

Wakefield can be roughly divided into resistive wall wakefield and structural wakefield. The structural wakefield mainly comes from the special pipe structure and the surface roughness during beam transportation, and the resistive wall wakefield primarily originates from different metal materials with different conductivity[12]. As bunch length σ_z and pipe radius a become shorter, the resistive wall wake is necessarily taken into consideration[13].

There are three pipes in SXFEL, with tiny σ_z and a, and opposite in pipe length. we neglect the surface bumps on the pipe, and simply consider the resistive wall wakefield. Furthermore, the wakefields in RF linac section have been studied carefully during beam dynamics simulation[10], thus we concentrate on the resistive wall wakefield from the end of linac to the exit of undulator part. Parameters of the three pipes are shown in Table 1.

Table 1 Parameters of three different types of pipes

	material	type	length/m	radius/mm
bypass-line 1	stainless-steel	round	125	17.50
bypass-line 2	stainless-steel	round	120	8.00
undulator	copper	flat plate	40	2.15

The short-range resistive wall wake function in a round, stainless-steel pipe is[14-15]

$$w_\delta(s)=\frac{4Z_0c}{\pi a^2}\left(\frac{1}{3}\mathrm{e}^{-\frac{s}{s_0}}\cos\left(\frac{\sqrt{3}s}{s_0}\right)-\frac{\frac{\sqrt{2}}{\pi}\int_0^\infty \mathrm{d}x x^2\mathrm{e}^{-\frac{sx^2}{s_0}}}{x^6+8}\right) \tag{1}$$

$$s_0=(2a^2/Z_0\sigma_c)^{1/3}$$

where s (>0) is the distance the test particle follows behind the drive particle, c is the speed of light, $Z_0=377\ \Omega$, a for pipe radius, s_0 for the characteristic distance which relates to the pipe radius and the conductivity σ_c. The resistive wall wakefield is easily got by the wake function $w_\delta(s)$ convolved with the bunch distribution $\lambda(s)$.

$$W_\delta(s)=\int_0^s \lambda(s-s')w_\delta(s)\mathrm{d}s' \tag{2}$$

The amplitude of wake function is mainly controlled by $\frac{4Z_0c}{\pi a^2}\left(\frac{1}{3}\mathrm{e}^{-s/s_0}\right)$, and period of wake function is controlled by $\cos(\sqrt{3}s/s_0)$. As seen in amplitude and period, both of them are affected by the radius and conductivity of the pipe. Apparently, considering the transitivity in convolution, the wakefields in different radius and conductivity will show different characteristics within the bunch length.

Typically, the current always operates at 1 kA for SXFEL, so 0.5 ps uniform distribution bunch with 1.35 GeV and 500 pC is suitably adopted to convolve with the wake function in bypass-lines 1and 2, and the results are shown in Fig.2. Due to the characteristic

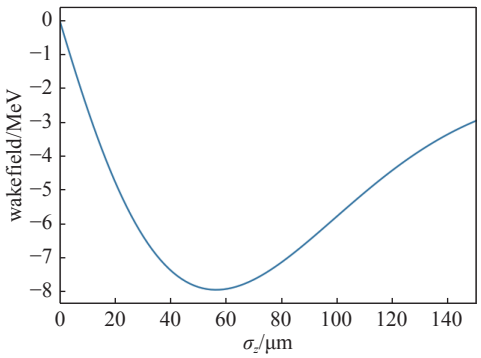

Fig. 2 Total wakefield in the bypass-line 1 and bypass-line 2. σ_z= 0 represents the head of the bunch, and the y-axis represents wakefield in MeV unit

of the convolution function, the resistive wall wakefield introduces a linear chirp of about 16 MeV/μm, reaching maximum value nearly 8 MeV at the position of 50 μm.

As shown in Table1, the SXFEL undulator beamline is equipped in vacuum undulator shielded with copper plate. Since the resistive wall wake function in a flat plate has the same gap, the maximum value of resistive wall wakefield is only $\pi^2/16$ times that of the round pipe[13]. Eq. (3) gives the impedance calculation formula of copper[16], where k represents the wave number, ω is the angular frequency, c is the speed of light, l is the mean free path of the conducted electrons, and $v_F$is the Fermi velocity. Adopting the parameters for the surface impedance, we numerically calculate impedance as a function of k ($Z(k)$) for copper.

$$\begin{cases} k = \omega/c \\ u^* = 1 - \mathrm{i}\omega l/v_F \\ \delta^{NSE} = \sqrt{\dfrac{2c}{Z_0\sigma_c\omega}} \\ \xi = \dfrac{(1-\mathrm{i})\omega\delta^{NSE}\sqrt{u}}{2c} \\ Z(k) = \dfrac{Z_0}{2\pi a}\displaystyle\int_0^\infty \frac{\mathrm{d}q}{\cosh(q)}\left[\frac{\cosh(q)}{\xi(k)} - \frac{\mathrm{i}ka}{q}\sinh(q)\right]^{-1} \end{cases} \tag{3}$$

The wakefield in the copper pipe is shown in Eq. (4), which is obtained by Fourier transform of the impedance convolved with the density distribution.

$$W_\delta(s) = \frac{c}{2\pi}\int_0^s \lambda(s)\int_{-\infty}^{\infty} Z(k)\mathrm{e}^{-\mathrm{i}k(s-s')}\mathrm{d}k\mathrm{d}s' \tag{4}$$

Adopting the same uniform bunch as the round pipe, the resistive wall wakefield of the copper flat-plate is shown on Fig.3. The wakefield oscillates as the cosine function and attenuates with period in 1/8 bunch length till the end of the bunch, corresponding to the resonant-like character in the impedance.

Comparing the round and flat-plate pipes, the total round pipe length is nearly 4 times that of the flat-plate pipe, and the radius of the flat-plate pipe is 4 times the round pipe radius. Consequently, the maximum wakefields effects in these two parts are 8 MeV and 4 MeV respectively, and the whole wakefield effects are obtained in Fig.4. The wakefields in different periods and amplitudes generate non-linearity, which eventually causes nearly 1% deterioration of the energy spread in SXFEL.

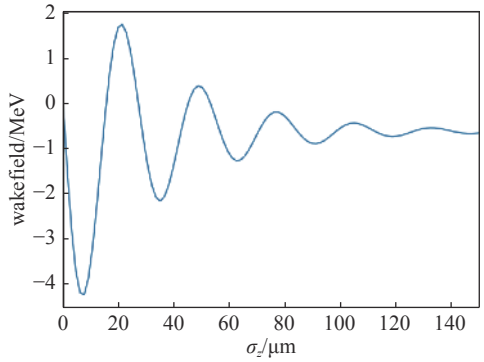

Fig. 3 Wakefield in the copper flat-plate pipe. The σ_z= 0 represents the head of the bunch, and the y-axis represents wakefield in MeV unit

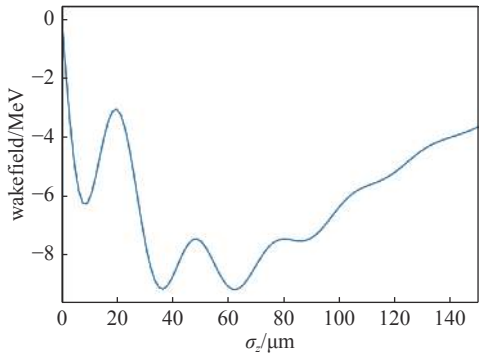

Fig. 4 Total wakefield for bypass-line 1, bypass-line 2 and the copper flat-plate pipe. σ_z= 0 represents the head of the bunch, and y-axis represents wakefield in MeV unit

2 Beam test experiment on SXFEL

2.1 Wakefield in bypass-line 1

The beam experiment was done on SXFEL, and the beam phase space is measured as shown in the right-bottom inset in Fig.5. The beam longitudinal distribution in SXFEL is obtained with an RF transverse cavity (TCAV) at the measurement location, named separately as TCAV1, TCAV2 and TCAV3, which gives the beam a time-dependent angular kick. Then, a dispersion element turns the longitudinal distribution information to transverse beam direction on the screens.

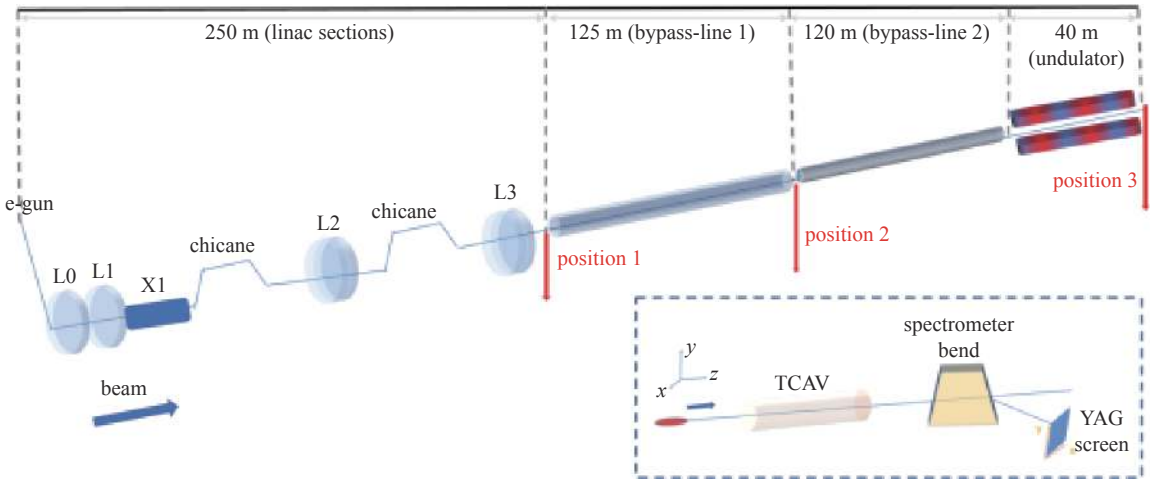

Fig. 5 Experimental layout of SXFEL

Table 2 gives the measured SXFEL bunch parameters at the exit of the linac (position 1). The Bunch A, a Gaussian-like distribution is shown in Fig.6(a) and adopted only for the wakefield calculation in 125 m bypass-line 1. Keeping the energy and charge constant, we change the accelerating phase in the linac and compress to a shorter bunch called as Bunch B. The double-horn distribution in Bunch B generated by the non-linear effects during bunch compression is utilized for detecting all the three pipes wakefields in Table 1.

Table 2 Initial bunch parameters in SXFEL

	length/μm	energy /GeV	charge/pC
bunch A	250	1.35	500
bunch B	120	1.35	500

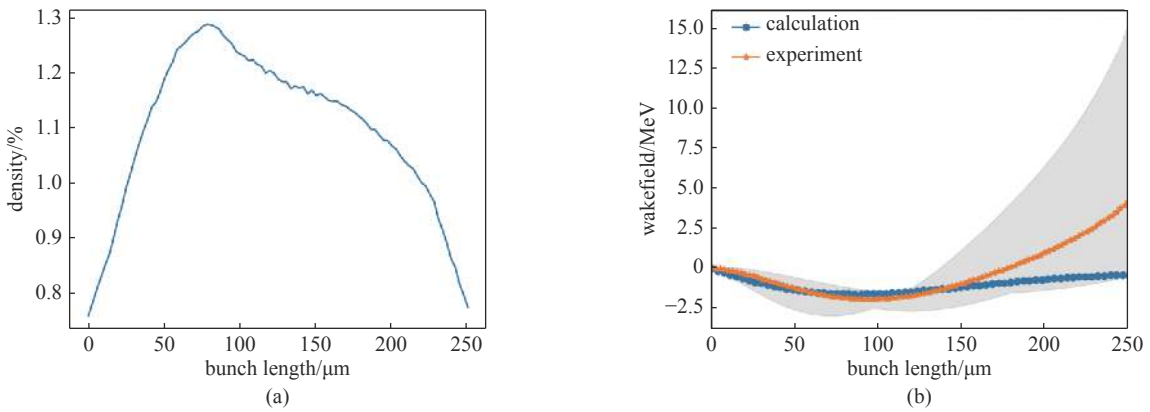

Fig. 6 (a) Distribution for bunch A, and (b) measured and calculated wakefields in bypass-line 1

The beam longitudinal phase space images at the end of the linac and the exit of the undulator measured at the YAG screen downstream of the energy spectrometer with TCAV 1 and TCAV 2 on are demonstrated in Fig.7. The average longitudinal wakefield in five times produced by the bypass-line 1 is shown in Fig.6(b) (the orange line), which is obtained by calculating the energy differences between Fig.7(a) and Fig.7(b) (there are still 4 sets of data not shown on position 2), and the grey area covers the maximum and minimum wakefields obtained in five times. The simulated wakefield (the blue line) by convolving the beam longitudinal distribution in position 1 with the wake function as mentioned in Eq. (1), is in reasonably good agreement with measurement. It is worth pointing that the difference in calculation and experiment mainly comes from the low signal-to-noise ratio, especially for the limited number of particles in the head of the bunch. Moreover, the discrepancy of the beam tail also comes from the beam position offset in transverse wake effect.

2.2 wakefield in all three pipes

Turning TCAV 1 and TCAV 3 on, respectively, the beam longitudinal phase space before and after the 3 pipes are separately demonstrated on Fig.8(a) and Fig.8(b).

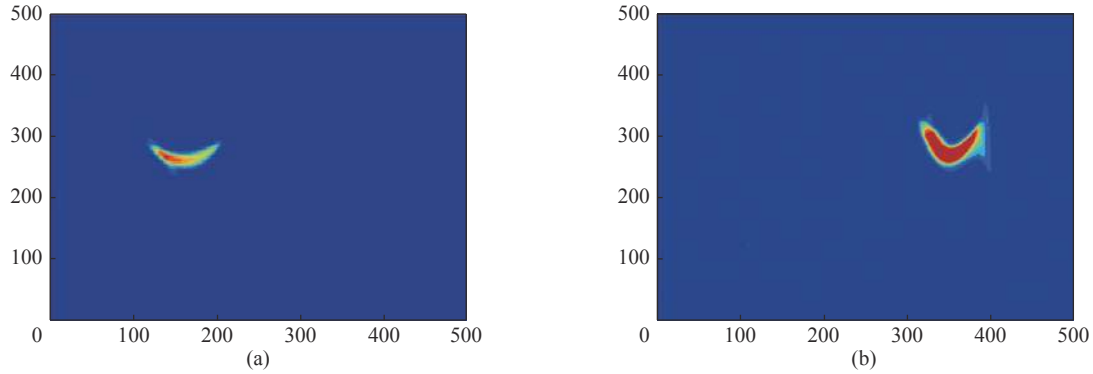

Fig. 7 Measured longitudinal phase space in position 1 and position 2. The figure is separated in 500×500 pixels, and x axis stands for bunch length (left is beam head), y stands for the energy (top is higher energy)

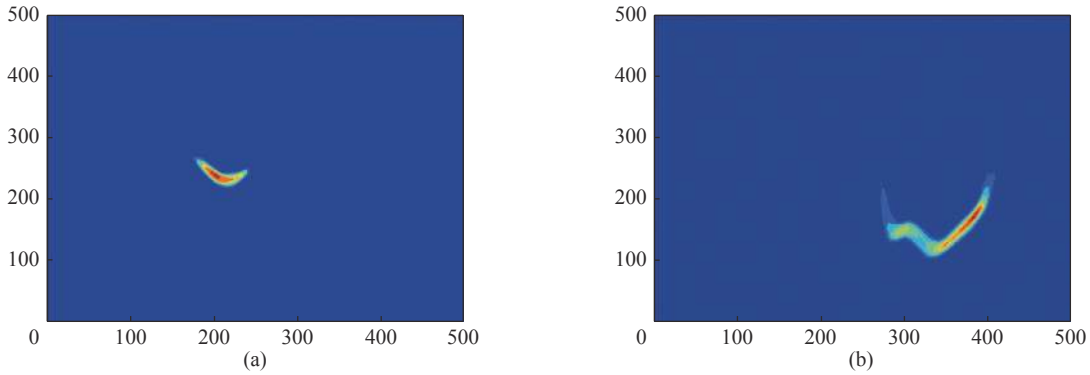

Fig. 8 The energy distribution in position 1 and position 3

Analyzing the energy differences between Fig.8(a) and Fig.8(b), the longitudinal wakefield produced by all the pipes is shown in Fig.9(b), in which w stands for the wakefield compared with the average energy in bunch. The simulated wakefield by convolving the bunch B distribution (Fig.9(a)) in position 1 with the wake function as mentioned in Eq. (1) and Eq. (4), shows great consistency with measurement. The largest difference between the calculation and experiment is observed at 80—100 μm, almost 0.5% of the total energy. The discrepancy is dependent on two statistical resolution methods for counting particles. The number of counting the background particles can affect the shape of bunch distribution, especially for the head and tail with lower numbers. The other factor is decided on the threshold value which can easily determine the location of the double-horn within the entire bunch distribution. Also as shown in last section, the consistency in beam tail suffers from the beam position offset from transverse wake effect.

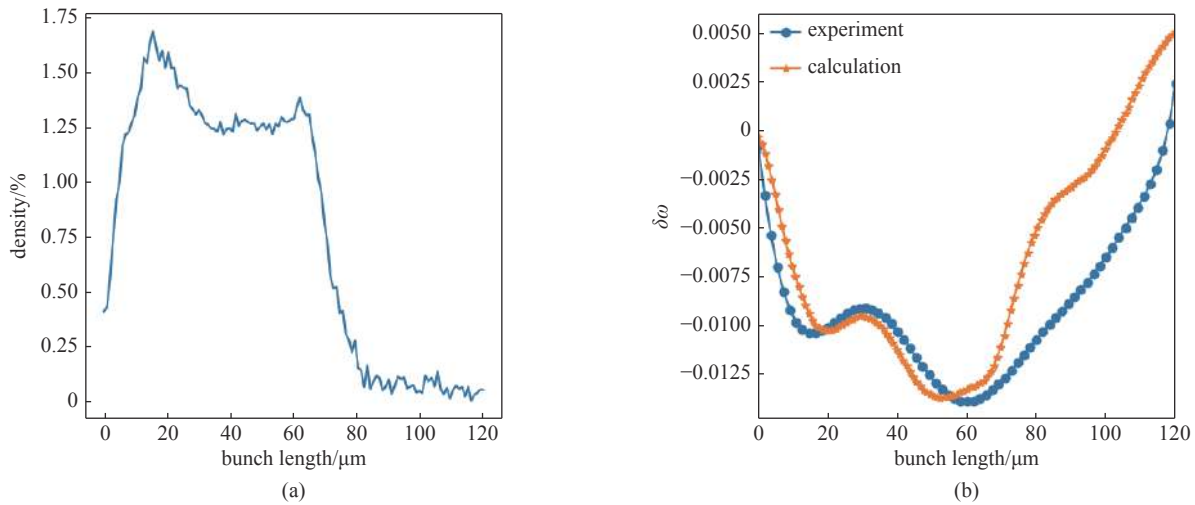

Fig. 9 (a) Distribution for bunch B and (b) measured and calculated wakefields for all the pipes

3 Conclusion

In this paper, we systematically investigated the effects of the resistive wall wakefields generated by the metal pipe from the end of RF linac section to the exit of undulator section. We calculated the resistive wall wakefield effects using uniform bunches and verified the distortion on the longitudinal phase space within each bunch. Detailed parameters of SXFEL were measured and further verified the wakefields effect by the round pipe and the whole pipe separately. Finally, we compared the measurement data with the wakefield calculated by the SXFEL bunch distribution and obtained great consistency. Analyzing the energy distortion caused by the resistive wall wakefield of SXFEL for the first time, this study can provide an instruction for the SXFEL linac beam optimization.

Reference:

[1] Kim K J. Brightness, coherence and propagation characteristics of synchrotron radiation[J]. Nuclear Instruments and Methods in Physics Research Section A:Accelerators, Spectrometers, Detectors and Associated Equipment, 1986, 246(1/3): 71-76.

[2] Öström H, Öberg H, Xin H, et al. Probing the transition state region in catalytic CO oxidation on Ru[J]. Science, 2015, 347(6225): 978-982.

[3] Young L, Kanter E P, Krässig B, et al. Femtosecond electronic response of atoms to ultra-intense X-rays[J]. Nature, 2010, 466(7302): 56-61.

[4] Liu Hailin, Hu Jie, Jiang Lan, et al. Ultrabroad antireflection urchin-like array through synergy of inverse fabrications by femtosecond laser-tuned chemical process[J]. Applied Surface Science, 2020, 528: 146804.

[5] Cheng C H, Li Ming. Nanometer material processing using NSOM-delivered femtosecond laser pulses[J]. MRS Online Proceedings Library, 2004, 850(1): 104-109.

[6] Geng Heping, Chen Jiahui, Zhao Zhentang. Scheme for generating 1 nm X-ray beams carrying orbital angular momentum at the SXFEL[J]. Nuclear Science and Techniques, 2020, 31(9): 88.

[7] Wang Jinguo, Liu Bo. Development of readout electronics for bunch arrival-time monitor system at SXFEL[J]. Nuclear Science and Techniques, 2019, 30: 82.

[8] Xiao Chengcheng, Zhang Junqiang, Tan Jianhao, et al. Design and preliminary test of the LLRF in C band high-gradient test facility for SXFEL[J]. Nuclear Science and Techniques, 2020, 31: 100.

[9] Huang Nanshun, Deng Haixiao, Liu Bo, et al. Features and futures of X-ray free-electron lasers[J]. The Innovation, 2021, 2: 100097.

[10] Zhao Zhentang, Wang Dong, Yin Lixin, et al. Shanghai soft X-ray free-electron laser facility[J]. Chinese Journal of Lasers, 2019, 46: 0100004.

[11] Zhao Zhentang, Wang Dong, Gu Qiang, et al. Status of the SXFEL facility[J]. Applied Sciences, 2017, 7: 607.

[12] Chao A W. Physics of collective beam instabilities in high energy accelerators[M]. New York: Wiley, 1993.

[13] Bane K L F. Wakefields of sub-picosecond electron bunches[R]. Report No. SLAC-PUB-11829, 2006.

[14] Bane K L F, Sands M. The short-range resistive wall wakefields[J]. AIP Conference Proceedings, 1996, 367(1): 131-149.

[15] Bane K, Raubenheimer T. Raubenheimer. Wakefield effects of the bypass line in the LCLS-II[R]. Report No. SLAC-PUB-16142, 2014.

[16] Stupakov G, Bane K L F, Emma P, et al. Resistive wall wakefields of short bunches at cryogenic temperatures[J]. Physical Review Accelerators and Beams, 2015, 18: 034402.

SXFEL 阻抗壁尾场对束流相空间畸变的影响

龚有为[1,2]， 程文才[1,2]， 赵明华[1]， 李 烜[3]， 谷 端[3]， 张 猛[3]

（1. 中国科学院 上海应用物理研究所，上海 201800； 2. 中国科学院大学，北京 100049； 3. 中国科学院 上海高等研究院，上海 201210）

摘 要： X 射线自由电子激光器（FEL）由于其超高亮度、超短脉冲等特点，在世界范围内得到广泛应用。基于尾流场理论，我们计算了上海 X 射线自由电子激光器（SXFEL）中从直线加速器出口到波荡器末端，束流在 245 m 不锈钢传输线和波荡器中的阻抗壁尾场。通过对两种不同的阻抗壁尾场的叠加，发现将导致束流纵向相空间的畸变。在 SXFEL 上进行束流物理的实验，并得到与理论预测非常吻合的实验结果。结合之前对主要直线加速器部分的详细模拟和实验研究，为后续 FEL 整体束流优化提供了参考。

关 键 词： 上海软 X 射线自由电子激光；纵向相空间；阻抗壁尾场；能量分布畸变